Placenta 88 (2019) 44–51

Contents lists available at ScienceDirect

Placenta

journal homepage: http://www.elsevier.com/locate/placenta

The porcine trophoblast cell line PTr2 is susceptible to porcine reproductive and respiratory syndrome virus-2 infection

M. Suleman [a,d], C.M. Malgarin [a], S.E. Detmer [b], J.C.S. Harding [a], D.J. MacPhee [c,*]

[a] Department of Large Animal Clinical Sciences, Western College of Veterinary Medicine, University of Saskatchewan, Saskatoon, SK, Canada
[b] Department of Veterinary Pathology, Western College of Veterinary Medicine, University of Saskatchewan, Saskatoon, SK, Canada
[c] Department of Veterinary Biomedical Sciences, Western College of Veterinary Medicine, University of Saskatchewan, Saskatoon, SK, Canada
[d] Department of Microbiology, Faculty of Veterinary Sciences, University of Veterinary and Animal Sciences, Lahore, Pakistan

ARTICLE INFO

Keywords:
Swine
PRRSV
Trophoblast
Maternal-fetal interface
Transmission

ABSTRACT

Introduction: Porcine reproductive and respiratory syndrome virus-2 (PRRSV-2) breaches the maternal-fetal interface (MFI) to infect porcine fetuses, yet the exact mechanism(s) of transmission is not understood. The objective of this study was to determine the susceptibility of porcine trophoblast cell line (PTr2) to PRRSV-2 infection to understand the potential role of the trophoblast in viral transmission to fetuses in vivo.

Methods: PTr2 cells were exposed in vitro to PRRSV-2 and then subjected to immunofluorescence analysis (IF), flow cytometry (FCM), real-time quantitative PCR (RT-qPCR), transmission electron microscopy (TEM) and immunogold electron microscopy (IEM) to assess viral infection. The effects of PRRSV-2 on PTr2 cell cycle progression and apoptosis, as well as the ability of PTr2 cells to produce infectious viral particles were also examined.

Results: PRRSV-2 was readily detected in PTr2 cells by IF, FCM, RT-qPCR, TEM and IEM techniques. RT-qPCR and FCM results of a time course of infection of PTr2 cells indicated PRRSV-2 load decreased over time after initial infection up to 72 h. PRRSV-2 infection altered PTr2 cell cycle with a selective increase of cells within the G2/M phase and also induced apoptosis. TEM and IEM demonstrated PRRSV-2 within and on the surface of PTr2 cells and PRRSV-2 virions released from PTr2 cells infected naïve MARC-145 cells inducing cytopathic effects.

Discussion: Trophoblast cells are susceptible to PRRSV-2 infection and release live virions capable of inducing cytopathic effects in naïve cells. This suggests a possible mechanism by which PRRSV-2 can breach the MFI resulting in fetal infection and death.

1. Introduction

Porcine reproductive and respiratory syndrome virus 2 (PRRSV-2) is an enveloped, positive strand RNA virus [1]. It is capable of breaching the maternal-fetal interface (MFI) leading to reproductive failure, including abortions, fetal mummification, and congenital infections [2]. The syndrome is one of the most economically damaging diseases in swine within North America with Holtkamp and colleagues estimating a total annual cost of productivity losses in the US national breeding and growing-pig herd of $664 million dollars [3]. Losses in the breeding herd at the time of their study accounted for 45% of the total cost of the syndrome [3].

The pig has non-invasive diffuse, epitheliochorial placentation with no decidualization of endometrium or invasion of fetal trophoblast into the maternal tissue in contrast to the discoid hemochorial human placenta [4]. Fertilization and a preimplantation period are followed by a peri-implantation stage from day (d)12–18 of gestation marked by rapid elongation of the trophoblast, release of 17β-estradiol as a maternal recognition of pregnancy signal, and trophoblast differentiation for attachment to uterine luminal epithelium starting at ~ d13-14 [5–7]. At sites of uterine glands, specialized trophoblast cell structures termed areolae also begin developing at ~ d15 to absorb uterine gland secretions [7].

The maternal endometrial epithelium and fetal trophoblast become tightly adhered and folding subsequently begins at ~ d30-35. The interdigitation becomes more extensive and complex with increasing gestation, although what controls the development of the folded bilayer

* Corresponding author. Department of Veterinary Biomedical Sciences, Western College of Veterinary Medicine, 52 Campus Dr, University of Saskatchewan, Saskatoon, SK, S7N 5B4, Canada.
E-mail address: d.macphee@usask.ca (D.J. MacPhee).

https://doi.org/10.1016/j.placenta.2019.10.004
Received 2 April 2019; Received in revised form 5 September 2019; Accepted 4 October 2019
Available online 5 October 2019

Nonstandard abbreviations

CPE	cytopathic effects
FBS	fetal bovine serum
MOI	multiplicity of infection
MFI	maternal-fetal interface
PRRSV-2	porcine reproductive and respiratory syndrome virus-2
PTr2	porcine trophoblast cell line
RT-qPCR	real time quantitative PCR

is still unclear [8]. Vallet and Freking [9] examined placentae from d45, 65, 85 and 105 of gestation using histology and morphometry. They reported increased width of the placental folds with increasing gestation. The length of the folds per unit of placental length increased in the same manner. Ultrastructural changes in the trophoblast and uterine epithelium also occur as pregnancy proceeds such as changes in cell height, extent of microvilli, and reduction of intervascular distance between maternal and fetal capillaries (~2 μm apart) to aid gas and solute exchange [10].

Placental trophoblast cells are designed, in part, to provide physical and immunological defenses against viruses [11]; however, many pathogens are known to breach the mammalian MFI to infect fetuses [12] including Zika virus and Hepatitis C virus in humans [13], as well as circovirus and parvovirus in pigs [14,15]. There is a lack of understanding of the exact mechanism(s) involved in PRRSV breaching of the MFI during porcine pregnancy, including the susceptibility of fetal trophoblast cells to PRRSV-2 infection [16].

Current data show PRRSV-1 localization and tropism towards macrophages as well as an increased number of sialoadhesin-positive and CD8-positive cells in the MFI associated with infection [17]. PRRSV-1 and -2 are involved in the induction of apoptosis during their replication in the MFI [18,19]. Multiple possible routes of viral transfer across the MFI have been postulated and recently published data suggest that non-cell associated mechanisms, such as free virions, may be involved in PRRSV-2 breaching of the MFI [20].

The main objective of the current study was to assess the susceptibility of a porcine trophoblast cell line (PTr2) to PRRSV-2 infection and then determine the effect of PRRSV-2 on PTr2 cell apoptosis, cell cycle progression, as well as the potential for viral release and transmission to a permissive cell line.

2. Material and methods

2.1. Cell lines and culture

The porcine trophoblast cell line PTr2 was kindly provided by Dr. Chandrakant Tayade (Queen's University, Kingston, ON, CA). The cell line was established from a d12 porcine conceptus and extensively characterized with detection of porcine trophoblast-specific interferon δ expression, cytokeratins such as cytokeratin 7, as well as immunoreactivity with SN1/38 porcine trophectoderm-specific monoclonal antibody [21]. PTr2 cultures were maintained in Dulbecco's Modified Eagle Medium/Nutrient Mixture F-12 (DMEM/F12; Cat # 21041–023, ThermoFisher Scientific, Burlington, ON, CA) supplemented with 5% charcoal stripped fetal bovine serum (Cat #F6765, Sigma-Aldrich, St. Louis, MO, USA), 0.1 Units/ml bovine insulin (Cat #I0516, Sigma-Aldrich), 2 mM glutamine (Cat # 25030–081, ThermoFisher), 100 U/ml penicillin and 100 μg/ml streptomycin (Cat # 15140–122, ThermoFisher). The monkey kidney cell line MARC-145 has been previously described [22]. MARC-145 cells were maintained in Modified Eagle Medium (MEM; Cat # 11095–080, ThermoFisher) supplemented with 7% heat-inactivated fetal bovine serum (Cat # 12483–020; ThermoFisher), 0.25 μg/ml fungizone (Cat # 15290–018, ThermoFisher), 100 U/ml penicillin and 100 μg/ml streptomycin (ThermoFisher). All cells were cultured at 37 °C in a humidified 5% CO_2 incubator.

2.2. PRRS virus propagation and titration

PRRSV-2 stocks (strain NVSL 97–7895; generously provided by Dr. R. Rowland, Kansas State University) were prepared by infecting a PRRSV permissive MARC-145 cell line at multiplicity of infection (MOI) of 0.1. Cytopathic effects (CPE) were observed at 24, 48 and 72 h post-infection. The culture was frozen at −80 °C after 72 h with 70–75% CPE and viral titration was conducted for calculating tissue culture infective dose 50 ($TCID_{50}$) as previously described [23].

2.3. Antibodies

Mouse monoclonal anti-PRRSV antibody (Cat # SDOW17; Rural Technologies, Inc. Brookings, SD, USA) was used for immunofluorescence (IF; 1:100 dilution) and for immunogold electron microscopy (IEM; 1:10 dilution). A non-specific mouse IgG (Cat # 015-000-003; Jackson ImmunoResearch, West Grove, PA, USA), used at the same concentration as the primary antiserum, was employed as a negative control in IF analysis and IEM. Goat anti-mouse antisera conjugated to Alexa Fluor (AF) 568 (Cat # A-21124, 1:400 dilution, ThermoFisher) and goat anti-mouse IgG conjugated to 15 nm gold particles (Cat # EM. GAM15, 1:100 dilution, BBI Solutions, Crumlin, UK) were utilized for IF and IEM, respectively.

2.4. Immunofluorescent staining of PRRSV-2

For IF analysis, PTr2 cells were infected at MOI of 1 and 5 and cultured for 24, 48, and 72 h in chamber slides. Cells were fixed in chilled methanol/acetone (1:1) for 10 min at −20 °C, air-dried, and washed twice in phosphate buffer saline (PBS). After blocking with 6% goat/3% donkey/1% fetal bovine serum in PBS for 1 h at room temperature, cells were incubated with anti-PRRSV antibody for 1 h at room temperature, washed four times in cold PBS with 0.02% Tween 20, and then incubated with secondary antibody for 1 h at room temperature. The slides were mounted with Prolong™ Diamond mounting media containing DAPI (Cat #P36966, ThermoFisher). Images were obtained using an Olympus® IX83 microscope system equipped with a high resolution Andor Zyla 4.2 sCMOS (2048 × 2048 pixel array) camera (Andor, Concord, MA, USA) and CellSens® imaging software (Olympus, Richmond Hill, ON, CA). Image conversion for analysis was conducted using ImageJ® (Ver. 1.50i).

2.5. Flow cytometry

Flow cytometry was used to assess PRRSV-2 infection of PTr2 cells. Following inoculation at MOI of 1 and 5 as described above, PTr2 cells were detached and fixed with 2% formaldehyde in PBS for 10 min. Cells were washed three times with PBS containing 0.1% Tween 20 and then immunostained for PRRSV using mouse monoclonal anti-PRRSV antibody and goat anti-mouse AF568-conjugated secondary antiserum. A FACSCalibur instrument (Becton Dickinson, Franklin Lakes, NJ, USA) was used for sample acquisition and 20,000 events were acquired with Cell Quest software (version 3.3). PTr2 cells were selected by utilizing a forward scatter/side scatter plot and gated to acquire maximum events since the cell line is a uniform population of epithelial cells. This was followed by plotting histograms for PRRSV-2-immunostained infected PTr2 cells. Positive immunostaining was established based on a mouse IgG isotype control. Data were subsequently analyzed using Kaluza (v. 1.3).

2.6. Quantification of PRRSV-2 RNA concentration

To quantify PRRSV-2 RNA concentrations, PTr2 cells infected at MOI

of 1 and 5 were collected for RNA isolation using an RNeasy MiniKit (Cat # 74106; Qiagen, Toronto, ON, CA) according to the manufacturer's instructions. Briefly, at the appropriate time points the culture supernatant was completely removed and 350 μl of lysis buffer was added to cells. Cell lysates were mixed by gentle pipetting to ensure that no cell clumps were visible before proceeding to subsequent steps. The final elution of samples was conducted using 25 μl of RNase-free water. For each experiment a known negative control was extracted simultaneously. Quantitative real time PCR (RT-qPCR) for PRRSV-2 was performed with 2 μl of samples as well as primers and reaction parameters that have been previously described in detail [24]. The results were reported as PRRSV RNA copies/μl.

2.7. Apoptosis assay

Apoptosis was detected in PTr2 cells using the single channel Annexin-V/Dead Cell Apoptosis kit for flow cytometry (Cat #V13240, ThermoFisher) according to the manufacturer's instructions. PTr2 cells were incubated with PRRSV-2 at MOI of 1 and 5 for 24, 48 and 72 h while Staurosporine-treated cells (20 μM) served as positive controls and untreated cells kept under the same culture conditions served as negative controls. After incubation, PTr2 cells were gently detached from culture plates using trypsin, washed twice with PBS, and suspended in 100 μl 1X freshly prepared Annexin-V binding buffer. Five microlitres of Annexin-V-AF488 and 2 μl of Sytox Green were added and cells were then kept at room temperature in the dark for 15 min. Following addition of 400 μl of Annexin-V binding buffer, cells were immediately analyzed with a BD FACSCalibur flow cytometer.

2.8. Cell cycle analysis

Cell cycle analysis was conducted using the Vybrant® DyeCycle™ Green kit (Cat #V35004, ThermoFisher) according to the manufacturer's instructions. PTr2 cells were incubated with PRRSV-2 at MOI of 1 and 5 for 24, 48 and 72 h. Untreated cells kept under the same culture conditions served as negative controls. Cells were detached from culture plates using trypsin, washed twice with PBS, and suspended in 1 ml of fresh culture medium. Two microlitres of Vybrant® DyeCycle™ Green stain was added to each cell suspension and cells were incubated in the dark at 37 °C for 30 min. Cells were then analyzed with a BD FACSCalibur flow cytometer at a low flow rate for acquisition.

2.9. Transmission electron microscopy (TEM)

PTr2 cells were infected at MOI of 1 and 5 for 72 h as described above and then cells were processed for TEM. Briefly, cells were fixed using a mixture of 2% paraformaldehyde/0.1% glutaraldehyde in cacodylate buffer, gently lifted from culture plates, and a cell pellet embedded in 1% low melting point agarose for processing. The cell pellet was dehydrated through a cold graded ethanol series (10 min per step) followed by three changes of 100% ethanol. Pellets were then embedded in LR White resin (Cat # 14381, Electron Microscopy Services, Halfield, PA, USA) as follows: ethanol:LR White 2:1, ethanol:LR White 1:1, ethanol:LR White 1:2 for 1 h each and then 100% LR White overnight. All embedded samples were polymerized in BEEM capsules under anaerobic conditions with a Blacklight Blue lamp at −20 °C for 3 days. Sections were placed on 200 mesh nickel grids, dried and stained before imaging.

2.10. Immunogold electron microscopy (IEM)

Sections of PTr2 cell pellets on nickel grids were blocked with 1% bovine serum albumin. Subsequently, the samples were incubated with anti-PRRSV antibody for 1 h at room temperature. Grids were rinsed in PBS followed by incubation with gold-conjugated secondary antibody for 1 h at room temperature. Grids were washed with PBS, distilled water and then stained with 2% aqueous uranyl acetate/0.1% Triton X-100 for 20 min followed by washes in distilled water. Excess water was blotted with tissue paper and grids incubated for 10 min with Reynolds lead citrate, followed by washes with distilled water. Samples were then observed with an Hitachi 7700 transmission electron microscope.

2.11. Assessment of PRRSV-2 release from PTr2 cells

To assess the ability of PTr2 cells to release live virus and infect permissive cells, PTr2 cells were infected at MOI of 5 and cultured for 24, 48 and 72 h (Supplementary Fig. 1). At each timepoint, cells were detached by trypsinization, washed 10 times with PBS, and plated in fresh media. The last PBS wash was retained as a control for assessment of viral carry over. The conditioned media was collected 24 h after the final plating for each post-infection time point to gather any PRRSV shed from infected PTr2 cells. The conditioned media collected from uninfected PTr2 cells served as a negative control for virus shedding. Five hundred microlitres of conditioned media from each culture or last PBS wash was then transferred to ~70% confluent naïve MARC-145 cells and the cells were further cultured for up to 7 days or until the development of any CPE was observed. Twenty four hours post-transfer to MARC-145 cells, media was collected for RT-qPCR to confirm the presence and concentration of PRRSV-2 that could subsequently induce CPE. Five hundred microlitres of the collected culture supernatant were added to RNeasy MiniKit lysis buffer and processed for RT-qPCR as described above. Phase contrast images of MARC-145 cells were obtained using an Olympus® IX83 microscope system equipped with a colour DP73 camera and Olympus CellSens® imaging software. The images were converted for analysis using ImageJ® (Ver. 1.50i).

2.12. Statistical analyses

Time course experiments examining PRRSV-2 infection and viral load of PTr2 and MARC-145 cells were assessed with one-way ANOVA followed by post-hoc Tukey multiple comparisons tests. Apoptosis and cell cycle analyses were assessed by two-way ANOVA followed by post-hoc Sidak multiple comparison tests. Statistical differences were considered significant at $P \leq 0.05$ *a priori*. Data were analyzed using GraphPad Prism 8 for Mac OS X (GraphPad Software, La Jolla, CA, USA, www.graphpad.com).

3. Results

3.1. PRRSV-2 infects PTr2 cells

To evaluate their susceptibility to PRRSV-2, PTr2 cells were inoculated with PRRSV-2 at MOI of 5 and cultured for 24, 48 and 72 h. Infected PTr2 cells exhibited mild CPE after 72 h post-infection indicating invasion and potential replication of PRRSV (Fig. 1A and B). Using IF analysis PRRSV-2 was detected in infected cells at all three time points examined (Fig. 1C and D).

To evaluate the percentage of infected PTr2 cells, cells infected with PRRSV-2 at MOI of 1 and 5 and incubated for 24, 48 and 72 h were quantified using flow cytometry. At MOI of 1, the percentage of PTr2 cells infected with PRRSV-2 was significantly lower at 72 h post-infection (4.65% ± 0.10) compared to 24 h (11.85% ± 0.10) and 48 h (8.32% ± 0.23; $P \leq 0.0001$; Fig. 1E). Furthermore, the percentage of infected cells was significantly lower at 48 h compared to 24 h ($P \leq 0.0001$). At MOI of 5, the percentage of PRRSV-2 infected cells was greater than at MOI of 1, but again the percentage of infected cells was significantly lower at 72 h (12.80% ± 0.28) compared to 24 h (31.10% ± 4.78) and 48 h (25.18% ± 4.15; $P \leq 0.0001$; Fig. 1E).

Evidence from IF and flow cytometry demonstrated that PTr2 cells were infected with PRRSV-2, thus RT-qPCR was conducted to precisely quantify the viral load in PTr2 cells at each time point post-infection. At MOI of 1 and 5 the PRRSV RNA concentration was significantly decreased at 72 h compared to 24 h ($P \leq 0.05$; Fig. 1F) indicating

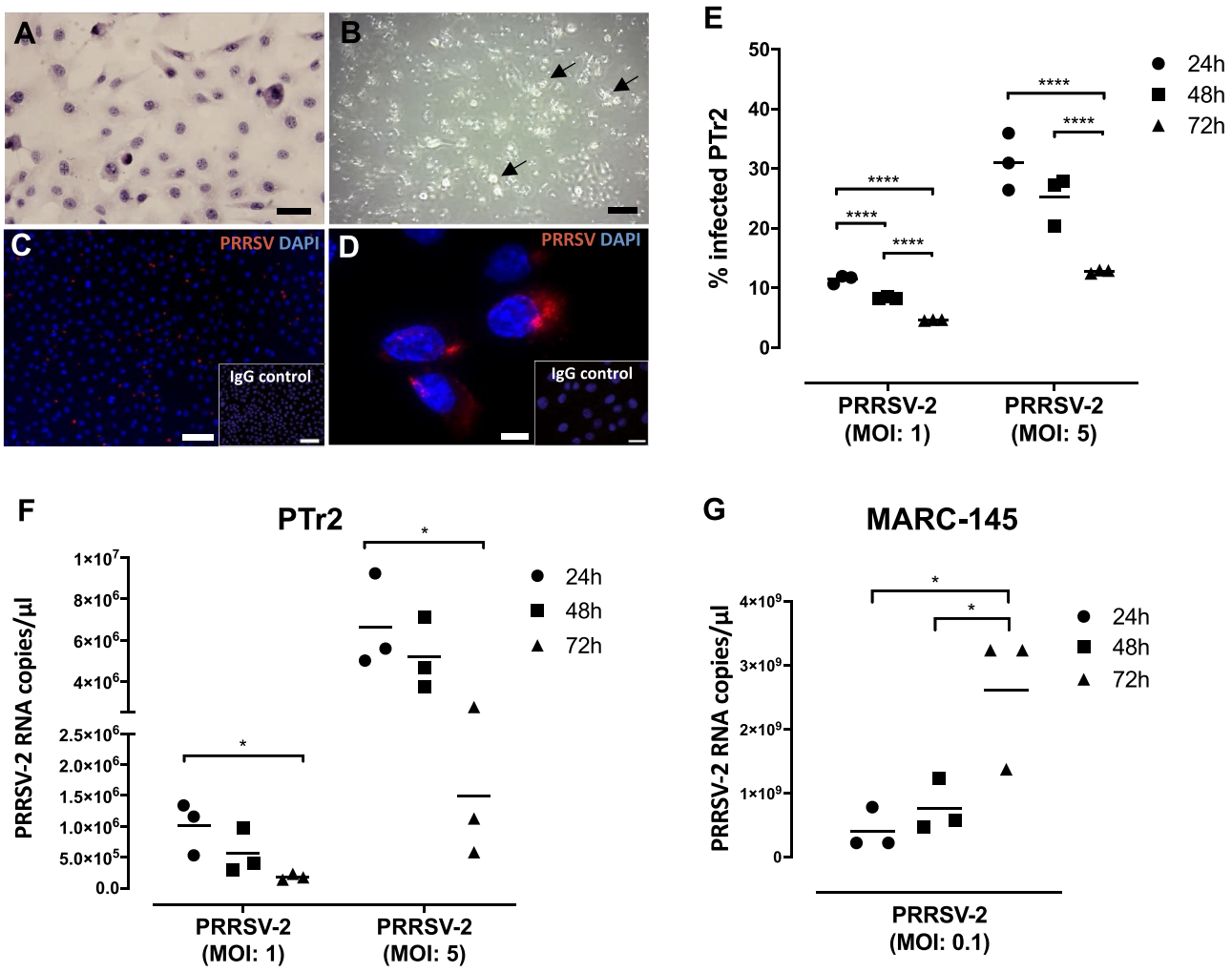

Fig. 1. PRRSV-2 detection and quantification in infected PTr2 cells. PTr2 cells were infected with PRSSV-2 at MOI of 5 and cultured for 72 h. A. H & E staining showing infected PTr2 cells; B. PRRSV-2-induced cytopathic effects in PTr2 cells, shown as partially rounded cells (black arrows); C. PRRSV-2 (red) was detected using immunofluorescence in infected PTr2 cells. DAPI-stained nuclei (blue) are also shown; D. Higher magnification of panel C showing PRRSV-2 detection within the PTr2 cells. Immunoglobulin (IgG) control images are shown within the insets. Scale bars: A = 50 µm; B, C and Inset of C = 100 µm; D = 10 µm and inset of D = 25 µm; E. Flow cytometry results of PRRSV-2 infected PTr2 cells at MOI of 1 and 5 following incubation for 24–72 h. The percentage of PRRSV-2 positive cells significantly decreased over time; F. RT-qPCR quantification of PRRSV-2 in PTr2 cells infected at MOI of 1 and 5 at 24–72 h post-infection. PRRSV-2 RNA concentration decreased in infected PTr2 cells over time; G. RT-qPCR quantification of PRRSV-2 in MARC-145 cells infected at MOI of 0.1. RT-qPCR demonstrated an increase in PRRSV-2 RNA concentration over time indicating viral replication. Each graph represents one of three independent experiments conducted in triplicate. Significant differences between time points are shown by $*P \leq 0.05$ and $****P \leq 0.0001$.

PRRSV-2 did not replicate during the period examined, but was potentially released from the cells over time. For comparison, the PRRSV-2 permissive cell line MARC-145 was infected with PRRSV-2 at MOI of 0.1. The viral load significantly increased at 72 h compared to 24 and 48 h post-infection ($P \leq 0.05$; Fig. 1G).

3.2. PRRSV induces apoptosis in infected PTr2 cells

To further understand the decrease in the percentage of PRRSV-2 infected cells over time post-infection, apoptosis assays were conducted with PTr2 cells infected at MOI of 1 and 5 and cultured for 24, 48 and 72 h. Compared to uninfected cells where detection of apoptosis was less than 4% over 24–72 h, PRRSV-2 infected PTr2 cells exhibited significantly increased apoptosis at both MOI tested. Specifically at MOI of 1, apoptosis was significantly elevated at 48 h and 72 h compared to uninfected cells ($P \leq 0.0001$). At MOI of 5, apoptosis was significantly elevated at 24 h ($P \leq 0.01$), as well as at 48 h and 72 h ($P \leq 0.0001$) compared to uninfected cells (Fig. 2). Staurosporine added to uninfected cells, to serve as a positive control, induced high levels of apoptosis in cells at all time points tested.

3.3. PRRSV-2 infection of PTr2 cells induces cell cycle alterations

Cell cycle analysis of PRRSV-2 infected PTr2 cells demonstrated that PRRSV-2 infection resulted in a significantly lower percentage of cells in G0/G1 at all timepoints and both MOI compared to uninfected cells ($P \leq 0.0001$, Fig. 3A–E). Conversely, higher percentages of infected cells were observed in G2/M phase compared to uninfected cells ($P \leq 0.0001$, Fig. 3A–D,G), while the percentages of cells in S phase were not significantly altered between uninfected and infected cells (Fig. 3A–D,F).

3.4. Ultrastructural localization of PRRSV-2 within PTr2 cells

Ultrastructural localization of PRRSV-2 within PTr2 cells was examined with TEM (Fig. 4). Uninfected cells exhibited a healthy and polarized side with mild apparent secretory activity (Fig. 4A), while

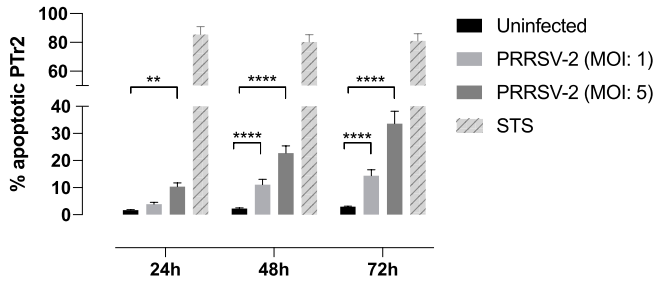

Fig. 2. PRRSV-2 infection induces apoptosis in PTr2 cells. PTr2 cells were infected with PRRSV-2 at MOI of 1 and 5 followed by culture for 24, 48 and 72 h. Apoptosis was measured using a commercial kit and flow cytometry. PRRSV-2 infected PTr2 cells exhibited significantly increased apoptosis at both MOI tested over time. Staurosporine (STS) added to uninfected cells, to serve as a positive control, induced high levels of apoptosis in cells at all time points tested. Data presented are mean percentages of apoptotic PTr2 cells (±SD) from one of three independent experiments conducted in triplicate. Significant differences between infected and uninfected cells at each time point are shown by $^{**}P < 0.01$ and $^{****}P < 0.0001$.

infected cells showed extensive secretory activity and budding (Fig. 4B). Putative localization of spherical PRRSV-2 virions of 55–75 nm was observed in both the cytoplasm and within vesicles (Fig. 4C). Putative enveloped virions also appeared to be released from the plasma membrane of some polarized infected cells (Fig. 4D–F).

3.5. Confirmation of PRRSV-2 presence in PTr2 cells with IEM

IEM was conducted to confirm the presence and localization of PRRSV-2 within infected PTr2 cells. PRRSV-2 specific immunogold labelling was observed in the cytoplasm of infected cells and also within vesicles (Fig. 5A–C). IEM also demonstrated PRRSV-2 specific immunogold labelling at sites of apparent secretory budding near the cell surface (Fig. 5D and E) indicating the possible route of PRRSV-2 release from infected PTr2 cells. The non-specific mouse IgG control demonstrated no immunogold labelling (Fig. 5F).

3.6. Release of PRRSV-2 from infected PTr2 cells

Based on the TEM and IEM analyses of infected PTr2 cells, the capacity of these cells to transfer infection to naïve PRRSV-2 susceptible MARC-145 cells was assessed. Infected PTr2 cells shed PRRSV-2 in culture supernatant following 24, 48 and 72 h of culture and the released virus infected recipient naïve MARC-145 cells resulting in CPE (Fig. 6A–C). Culture media supernatant from uninfected PTr2 cells was used as a negative control and produced no CPE in cells (Fig. 6D–F). PBS collected from the last (10th) wash of infected PTr2 cells was also transferred to naïve MARC-145 cells and no CPE were observed demonstrating no viral carry over of PRRSV-2 (Fig. 6G–I). The CPE

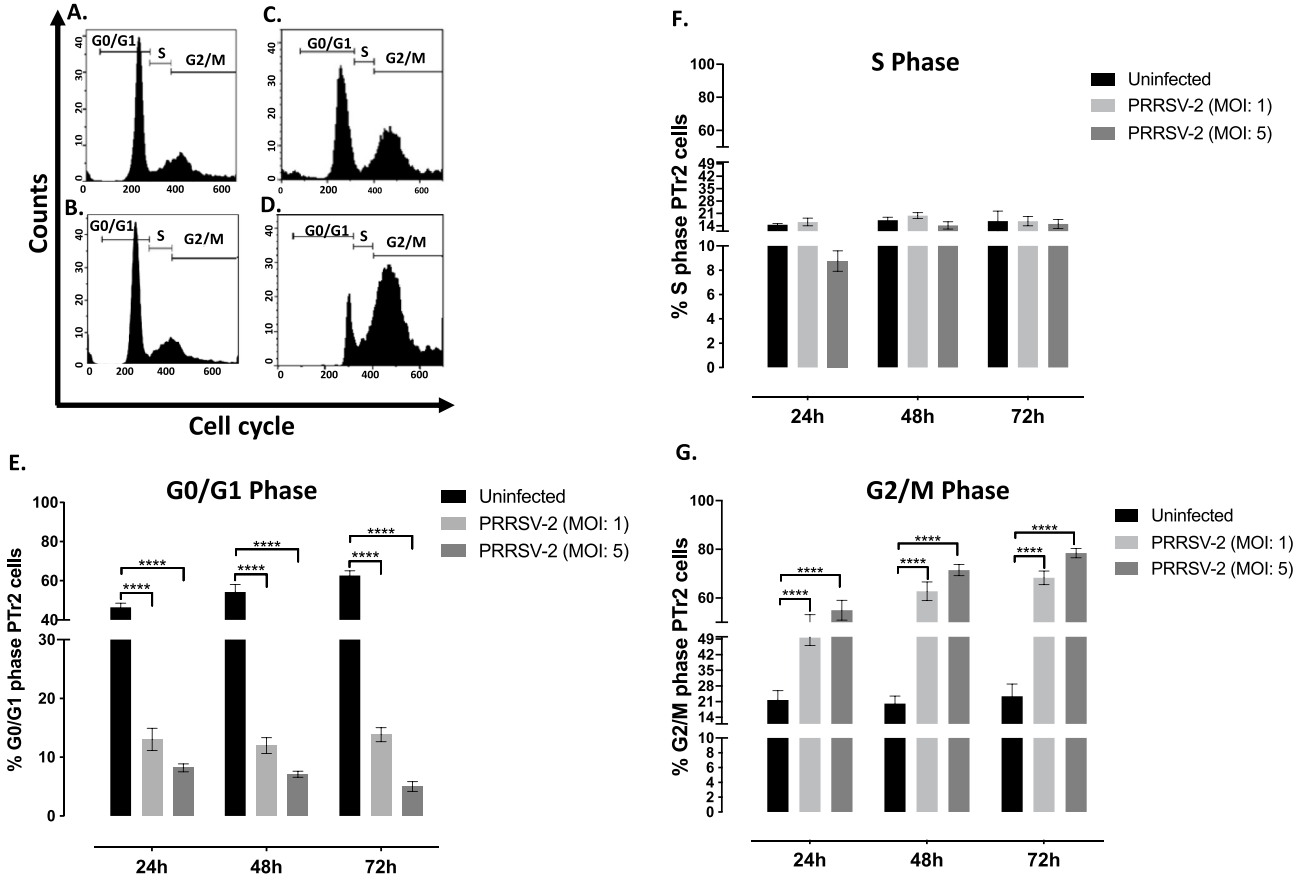

Fig. 3. PRRSV-2 induces alteration in cell cycle stages within infected PTr2 cells. PTr2 cells were infected with PRRSV-2 at MOI of 1 and 5 and grown for 24, 48 and 72 h. Cell cycle state was measured using a commercial kit and flow cytometry; A,B. Cell cycle stages of untreated cells at 24 and 48 h, respectively; C,D. Cell cycle stages of PRRSV-2 infected PTr2 cells (MOI of 5) at 24 and 48 h post-infection, respectively, demonstrating accumulation of PTr2 cells in the G2/M phase. Representative histograms of cell counts are shown; E-G. Quantitative analysis of uninfected and PRRSV-2 infected PTr2 cells in phases of the cell cycle. PRRSV-2 infection resulted in a significantly lower percentage of cells in G0/G1 phase at all timepoints and both MOI compared to uninfected cells. The percentages of cells in S phase were not significantly altered between uninfected and infected cells while higher percentages of infected cells were observed in G2/M phase compared to uninfected cells. Data shown are from one of three independent experiments conducted in triplicate. Bars represent means ± SD. Significant differences between uninfected and infected cells at each time point are shown by $^{****}P < 0.0001$.

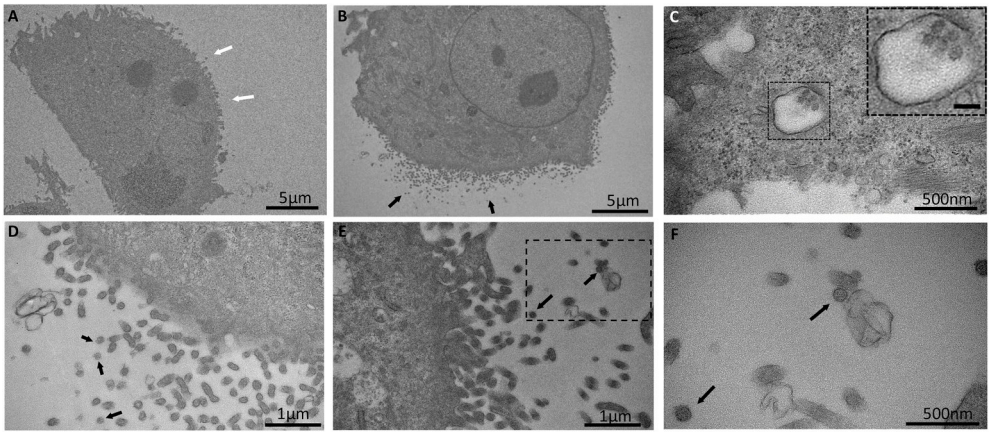

Fig. 4. Ultrastructural localization of PRRSV-2 in infected PTr2 cells using transmission electron microscopy (TEM). PTr2 cultures were infected with PRRSV-2 at MOI of 5 for 72 h and processed for TEM. A. Uninfected cell showing polarization and mild budding (white arrows); B. PRRSV-2 infected PTr2 cell showing extensive budding (black arrows); C. Infected PTr2 cells showing putative PRRSV-2 virions inside a vesicle (higher magnification shown in the inset, scale bar = 100 nm); D. Higher magnification of panel B showing putative PRRSV particles near the surface of infected PTr2 cells (black arrows); E. Infected PTr2 cell with shedding of putative PRRSV from the polarized surface (black arrows); F. Higher magnification of panel E (dotted box) showing putative viral particles in the vicinity of an infected cell. Images are representative of three independent experiments.

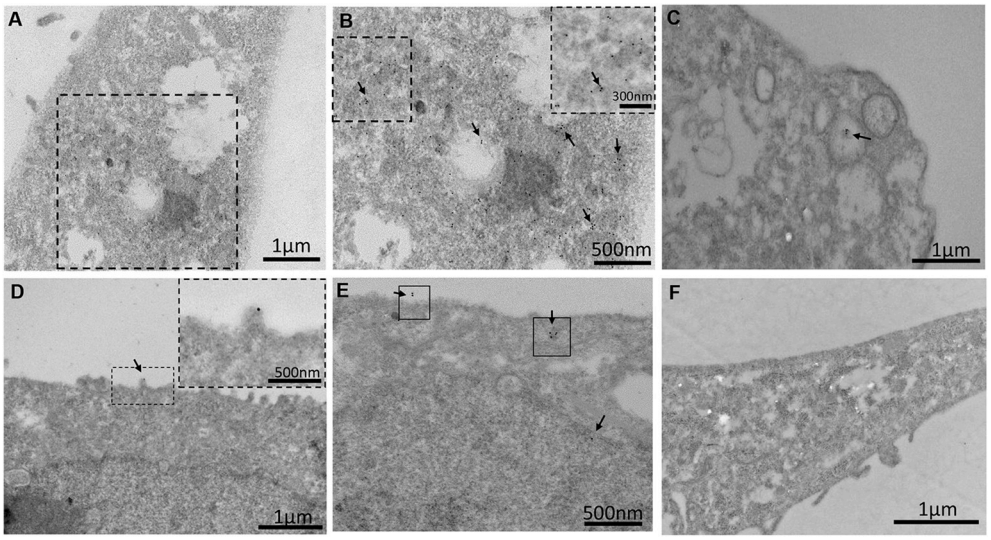

Fig. 5. PRRSV-2 presence in infected PTr2 cells demonstrated by immunogold electron microscopy (IEM). PTr2 cultures were infected with PRRSV-2 at MOI of 5 for 72 h and processed for IEM. A. Immunogold-stained PRRSV-2 within an infected PTr2 cell; B. Higher magnification of panel A (dotted box) showing multiple immunogold-stained PRRSV-2 particles (black arrows). A higher magnification is shown in the inset; C. A vesicle within a PRRSV-2-infected PTr2 cell with immunogold-stained PRRSV particles; D. Immunogold-labelled PRRSV-2 (arrow) in a putative secretory bud (dotted box) at the surface of the infected PTr2 cell. A higher magnification is shown in the inset; E. Immunogold-labelled PRRSV-2 (arrows) near the cell membrane (boxes); F. A non-specific IgG control demonstrating lack of immunogold labelling in infected PTr2 cells. Images are representative of three independent experiments.

results were validated using RT-qPCR. PRRSV-2 RNA was not detected in culture media supernatant from uninfected negative control recipient MARC-145 cells and last wash-exposed recipient MARC-145 cells, whereas PRRSV-2 RNA was detected in supernatant from recipient MARC-145 cells exposed to conditioned media from infected PTr2 (Fig. 6J).

4. Discussion

Three mechanisms of PRRSV-2 breaching across the MFI have been proposed: a migration of infected maternal macrophages across the MFI, a direct movement of free virus, or a cell-cell movement of virus into and through the intact maternal-fetal epithelial layers [16]. To better understand how PRRSV-2 could breach the porcine MFI during pregnancy, we investigated the possibility of trophoblast cells being susceptible to PRRSV-2 infection. Our results are supportive of the third mechanism.

We have recently reported the presence of non-cell associated PRRSV-2 viral antigens at the porcine MFI with a significant increase in small PRRSV-2 antigen spot counts observed at the fetal-maternal junction and placenta between 5 and 8 days post-infection [20]. Immunofluorescence analysis also detected some PRRSV-2 viral antigen between fetal trophoblast cells or beyond basal membranes of trophoblast cells suggestive of virion movement through or between the fetal trophoblast layer [20].

Using IF and IEM, our current study has clearly demonstrated detection of PRRSV-2 in PTr2 cells at all time points examined post-infection. The percentage of PRRSV-2 positive cells decreased in infected PTr2 cells over time, which could be a result of infection-mediated cell lysis, but flow cytometry and RT-qPCR confirmed that PTr2 cells were susceptible to PRRSV infection and mild CPE were also observed. Thus, these data are the first in vitro evidence of porcine trophoblast cells being directly vulnerable to PRRSV-2 infection. Since the PTr2 cell line is derived from an elongated 12 day old porcine conceptus [21], we cannot be certain that the susceptibility to infection will be similar in trophoblast later in gestation as trophoblast cells do undergo ultrastructural changes during pregnancy [10]. Trophoblast-endometrial attachment certainly facilitates PRRSV infection as Prieto and colleagues [25] previously demonstrated that transplacental infection of PRRSV and embryonic death can occur at day 20 of gestation (not day 10) when trophoblast-endometrial attachment has recently occurred, but the bilayer has not begun to interdigitate [8]. Kranker et al. [26] also found PRRSV crosses the placental barrier at day 72 and 85 of gestation when the placental bilayer is highly folded and the distance between fetal and maternal capillaries is small [8]. However, porcine trophoblast cells from the peri-implantation period onwards, possess the ultrastructural features necessary for secretion and absorption [5,10,27] and

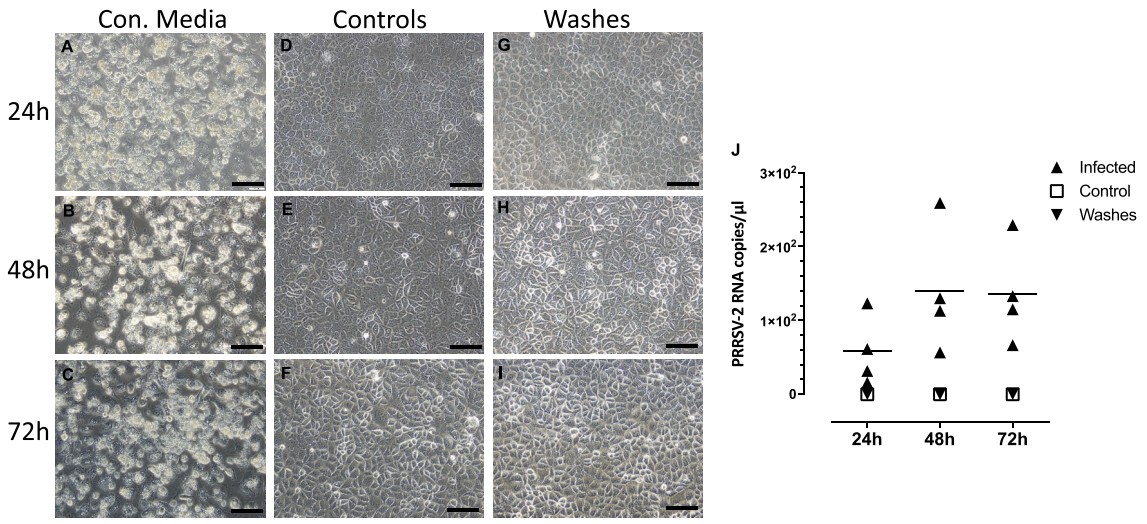

Fig. 6. Infected PTr2 cells are capable of transferring infection to naïve MARC-145 cells. PTr2 cultures were infected with PRRSV-2 at MOI of 5 and cultured for 24, 48 or 72 h. Cells were detached at each time point and washed 10 times with PBS. Washed PTr2 cells were then plated and further incubated 24 h before collection of conditioned media, which were added to naïve MARC-145 cells. A-C. Recipient MARC-145 cells exposed to conditioned media (Con. Media) from PTr2 cells infected for 24, 48 or 72 h demonstrated PRRSV-2 induced cytopathic effects (CPE) following culture for up to 7 days; D-F. MARC-145 cells cultured for a similar time in conditioned media from uninfected PTr2 cells (Controls) showed no CPE; G-I. MARC-145 cells incubated with the last PBS wash showed no CPE; Scale bars = 100 µm. J. RT-qPCR analysis of PRRSV-2 in culture media supernatant obtained 24 h post-transfer from infected, uninfected control, and last wash-exposed MARC-145 cells. PRRSV-2 RNA was only detected in supernatant from MARC-145 cells exposed to conditioned media from infected PTr2 cells. Data shown are from one of three independent experiments.

these processes could play a role in the uptake and/or transfer of free virions by trophoblast during pregnancy even before endometrial attachment is completed. A direct assessment of any differences in susceptibility of porcine trophoblast cells to infection at different periods of gestation is warranted.

PRRSV-2 viral load in PTr2 cells decreased from 24 h to 72 h post-infection suggesting PRRSV-2 was not replicating in these cells, but we cannot rule out PRRSV-2 replication at earlier timepoints. However, examination of PTr2 cell cycle characteristics and apoptosis post-infection showed that infected PTr2 cell populations undergo cell cycle arrest at G2/M phase by 24 h post-infection and some apoptosis compared to uninfected control cells. Mild CPE with considerable apoptosis is not unprecedented following PRRSV-2 infection as demonstrated in the porcine lung epithelial cell line SJPL by Provost and colleagues [28]. It is known that PRRSV-induced apoptosis is viral-replication dependent and stimulated, at least in part, by PRRSV nonstructural protein 4 and 10 [19,29,30]. In addition, PRRSV-2 induced apoptosis has been previously reported in the porcine MFI and cell lines including MARC-145 [18,19,31,32] and it is possible that soluble factors are produced by infected PTr2 cells to induce more widespread apoptosis initiation. Decreasing viral burdens over time post-infection could also be a result of the PTr2 cells combating the PRRSV infection. Even as early as day 12 of porcine gestation, trophoblast secrete interferons such as IFN gamma [33,34] and if secreted by PTr2 cells may slow or even inhibit viral replication. With respect to the cell cycle, viral infection, viral protein expression and even viral DNA presence can induce G2/M phase cell cycle arrest [35]. Cell cycle arrest influences PRRSV propagation as SJPL cells also exhibited inhibition of PRRSV replication upon infection with *Actinobacillus pleuropneumoniae* and G2/M phase arrest [36]. Thus, the observed decrease in viral load over time in PTr2 cells is likely a result of cell cycle arrest and death.

Using TEM and IEM we demonstrated the presence of PRRSV-2 particles inside membrane bound vesicles contained within PTr2 cells. Recently, the porcine chorioallantoic membrane and the PTr2 cell line were reported to produce extracellular vesicles including microvesicles and exosomes [37]. Such vesicles are known to transport RNA and microRNAs between cells [38]. Recently, Wang and colleagues [39] also showed that purified exosomes isolated from PRRSV-infected cells possessed viral genomic RNA and viral proteins. The presence of PRRSV-2 antigenic viral proteins in serum-derived exosomes from non-viremic animals that were previously exposed to PRRSV-2 has also been reported [40].

Using IEM, we observed PRRSV-2 on membrane sites at the surface of PTr2 cells suggesting the uptake and/or release of viral particles. We subsequently investigated whether or not PRRSV-2 could be released and transferred to naïve cells. Infected PTr2 cells released PRRSV-2 into cell culture supernatant and infected recipient naïve MARC-145 cells as demonstrated by observation of CPE. Thus, porcine trophoblast cells may facilitate PRRSV-2 transmission, at least in part, to the fetal side of the placenta. Previous work has shown that PRRSV distribution in the fetal placenta can be quite localized [19,20]. The limited infection of PTr2 cells observed in this study may also reflect an infection that is quite confined in nature and could subsequently result in localized transmission. Nonetheless, even limited localized infection over a large MFI could be sufficient for transfer to much more permissive macrophages on the fetal side of the placenta leading to robust replication and subsequent fetal infection.

A limitation of our study is the use of the PTr2 cell line derived from elongated, fetuses entering the peri-implantation stage that may not completely represent trophoblast at different gestational periods. For example, a large number of porcine genes have been reported to be differentially expressed during trophoblast elongation and subsequent trophoblast attachment to the uterine epithelium [6,8]. Nonetheless, our findings still provide novel evidence that our model of porcine trophoblast cells derived from 12 day old porcine conceptuses is susceptible to PRRSV-2 infection and can transfer virus to naïve cells. Our results suggest that virus transmission in vivo could involve virus transit through the dual epithelial layers either directly or by way of extracellular vesicles released from the surface of infected cells following cell cycle arrest and apoptosis.

Declaration of competing interest

The authors declared no potential conflicts of interest regarding the research, authorship, and publication of this article.

Acknowledgments

The authors acknowledge Larhonda Sobchishin for assistance with TEM and IEM processing and imaging as well as Dr. Chandrakant Tayade (Queen's University, Kingston, ON, CA) for providing the PTr2 cell line.

Appendix A. Supplementary data

Supplementary data to this article can be found online at https://doi.org/10.1016/j.placenta.2019.10.004.

Funding

This project was supported by grants from Genome Canada (Project # 345169) and Genome Prairie (Saskatchewan Ministry of Agriculture; Project # 20150329) and administrative support from Genome Alberta (Project #345169) and a Canada Foundation for Innovation John R. Evans Leaders Fund (Project # 32512).

References

[1] E.J. Snijder, W.J.M. Spaan, Arteriviruses, in: fifth ed., in: D.M. Knipe, P.M. Howley (Eds.), Fields Virology, vol. 1, Lippincott Williams & Wilkins, Philadelphia, 2007, 1337-1255.
[2] W.T. Christianson, C.S. Choi, J.E. Collins, T.W. Molitor, R.B. Morrison, H.S. Joo, Pathogenesis of porcine reproductive and respiratory syndrome virus infection in mid-gestation sows and fetuses, Can. J. Vet. Res. 57 (1993) 262–268.
[3] D.J. Holtkamp, J.B. Kliebenstein, E.J. Neumann, J.J. Zimmerman, H.F. Rotto, T. K. Yoder, C. Wang, P.E. Yeske, C.L. Mowrer, C.A. Haley, Assessment of the economic impact of porcine reproductive and respiratory syndrome virus on United States pork producers, J. Swine Health Prod. 21 (2013) 72–84.
[4] M. Bidarimath, C. Tayade, Pregnancy and spontaneous fetal loss: a pig perspective, Mol. Reprod. Dev. 84 (2017) 856–869.
[5] R.D. Geisert, J.W. Brookbank, R.M. Roberts, F.W. Bazer, Establishment of pregnancy in the pig: II. Cellular remodeling of the porcine blastocyst during elongation on day 12 of pregnancy, Biol. Reprod. 27 (1982) 941–955.
[6] J.W. Ross, M.D. Ashworth, D.R. Stein, O.P. Couture, C.K. Tuggle, R.D. Geisert, Identification of differential gene expression during porcine conceptus rapid trophoblastic elongation and attachment to uterine luminal epithelium, Physiol. Genom. 36 (2009) 140–148.
[7] J.L. Vallet, J.R. Miles, B.A. Freking, Development of the pig placenta, Soc. Reprod. Fertil. 66 (2009) 265–279.
[8] J.L. Vallet, A.K. McNeel, J.R. Miles, B.A. Freking, Placental accommodations for transport and metabolism during intra-uterine crowding in pigs, J. Anim. Sci. Biotechnol. 5 (2014) 55.
[9] J.L. Vallet, B.A. Freking, Differences in placental structure during gestation associated with large and small pig fetuses, J. Anim. Sci. 85 (2007) 3267–3275.
[10] A.E. Friess, F. Sinowatz, R. Skolek-Winnisch, W. Trautner, The placenta of the pig. I. Fine structural changes of the placental barrier during pregnancy, Anat. Embryol. 158 (1980) 179–191.
[11] A.I. Wells, C.B. Coyne, Type III interferons in antiviral defenses at barrier surfaces, Trends Immunol. 10 (2018) 848–858, https://doi.org/10.1016/j.it.2018.08.008.
[12] N. Arora, Y. Sadovsky, T.S. Dermody, C.B. Coyne, Microbial vertical transmission during human pregnancy, Cell Host Microbe 21 (2017) 561–567, https://doi.org/10.1016/j.chom.2017.04.007.
[13] L. Pereira, Congenital viral infection: traversing the uterine-placental interface, Annu. Rev. Virol. 5 (2018) 273–299, https://doi.org/10.1146/annurev-virology-092917-043236.
[14] J.S. Pittman, Reproductive failure associated with porcine circovirus type 2 in gilts, J. Swine Health Prod. 16 (2008) 144–148.
[15] A.L. Woods, E.J. McDowell, D. Holtkamp, R.M. Pogranichniy, T.G. Gillespie, Reproductive failure associated with porcine parvovirus and possible porcine circovirus type 2 co-infection, J. Swine Health Prod. 17 (2009) 210–216.
[16] U.U. Karniychuk, H.J. Nauwynck, Pathogenesis and prevention of placental and transplacental porcine reproductive and respiratory syndrome virus infection, Vet. Res. 44 (2013) 95, https://doi.org/10.1186/1297-9716-44-95.
[17] U.U. Karniychuk, W. De Spiegelaere, H.J. Nauwynck, Porcine reproductive and respiratory syndrome virus infection is associated with an increased number of Sn-positive and CD8-positive cells in the maternal–fetal interface, Virus Res. 176 (2013) 285–291, https://doi.org/10.1016/j.virusres.2013.05.005.
[18] P. Novakovic, J.C. Harding, A.N. Al-Dissi, S.E. Detmer, Type 2 porcine reproductive and respiratory syndrome virus infection increases apoptosis at the maternal-fetal interface in late gestation pregnant gilts, PLoS One 12 (2017), https://doi.org/10.1371/journal.pone.0173360 e0173360.
[19] U.U. Karniychuk, D. Saha, M. Geldhof, M. Vanhee, P. Cornillie, W. Van den Broeck, H.J. Nauwynck, Porcine reproductive and respiratory syndrome virus (PRRSV) causes apoptosis during its replication in fetal implantation sites, Microb. Pathog. 51 (2011) 194–202, https://doi.org/10.1016/j.micpath.2011.04.001.
[20] M. Suleman, P. Novakovic, C.M. Malgarin, S.E. Detmer, J.C.S. Harding, D. J. MacPhee, Spatiotemporal immunofluorescent evaluation of porcine reproductive and respiratory syndrome virus transmission across the maternal-fetal interface, Pathog. Dis. 76 (2018) fty060, https://doi.org/10.1093/femspd/fty060.
[21] L.A. Jaeger, A.K. Spiegel, N.H. Ing, G.A. Johnson, F.W. Bazer, R.C. Burghardt, Functional effects of transforming growth factor beta on adhesive properties of porcine trophectoderm, Endocrinology 146 (2005) 3933–3942.
[22] M. Ge, Y. Zhang, Y. Liu, T. Liu, F. Zeng, Propagation of field highly pathogenic porcine reproductive and respiratory syndrome virus in MARC-145 cells is promoted by cell apoptosis, Virus Res. 213 (2016) 322–331, https://doi.org/10.1016/j.virusres.2015.12.023.
[23] M. Suleman, S. Galea, F. Gavard, N. Merillon, B. Klonjkowski, E. Tartour, J. Richardson, Antigen encoded by vaccine vectors derived from human adenovirus serotype 5 is preferentially presented to CD8+ T lymphocytes by the CD8alpha+ dendritic cell subset, Vaccine 29 (2011) 5892–5903, https://doi.org/10.1016/j.vaccine.2011.06.071.
[24] P. Novakovic, S.E. Detmer, M. Suleman, C.M. Malgarin, D.J. MacPhee, J.C. S. Harding, Histologic changes associated with placental separation in gilts infected with porcine reproductive and respiratory syndrome virus, Vet. Pathol. 55 (2018) 521–530, https://doi.org/10.1177/0300985818765067.
[25] C. Prieto, P. Suárez, I. Simarro, C. García, A. Fernández, J.M. Castro, Transplacental infection following exposure of gilts to porcine reproductive and respiratory syndrome virus at the onset of gestation, Vet. Microbiol. 57 (1997) 301–311.
[26] S. Kranker, J. Nielsen, V. Bille-Hansen, A. Bøtner, Experimental inoculation of swine at various stages of gestation with a Danish isolate of porcine reproductive and respiratory syndrome virus (PRRSV), Vet. Microbiol. 61 (1998) 21–31.
[27] J. Ramsoondar, R.J. Christopherson, L.J. Guilbert, T.G. Wegmann, A porcine trophoblast cell line that secretes growth factors which stimulate porcine macrophages, Biol. Reprod. 49 (1993) 681–694.
[28] C. Provost, J.J. Jia, N. Music, C. Levesque, M.-E. Lebel, J. Re del Castillo, M. Jacques, C.A. Gagnon, Identification of a new cell line permissive to porcine reproductive and respiratory syndrome virus infection and replication which is phenotypically distinct from MARC-145 cell line, Virol. J. 9 (2012) 267.
[29] S. Costers, D.J. Lefebvre, P.L. Delputte, H.J. Nauwynck, Porcine reproductive and respiratory syndrome virus modulates apoptosis during replication in alveolar macrophages, Arch. Virol. 153 (2008) 1453–1465.
[30] S. Yuan, N. Zhang, L. Xu, L. Zhou, X. Ge, X. Guo, H. Yang, Induction of apoptosis by the nonstructural protein 4 and 10 of porcine reproductive and respiratory syndrome virus, PLoS One 11 (2016) e0156518.
[31] L.C. Miller, J.M. Fox, Apoptosis and porcine reproductive and respiratory syndrome virus, Vet. Immunol. Immunopathol. 102 (2004) 131–142.
[32] J.C.S. Harding, A. Ladinig, P. Novakovic, S.E. Detmer, J.M. Wilkinson, T. Yang, J. K. Lunney, G.S. Plastow, Novel insights into host responses and reproductive pathophysiology of porcine reproductive and respiratory syndrome caused by PRRSV-2, Vet. Microbiol. 209 (2017) 114–123, https://doi.org/10.1016/j.vetmic.2017.02.019.
[33] C. La Bonnardiere, J.-E. Flechon, S. Battegay, B. Flechon, J. Degrouard, F. Lefebvre, Polarized porcine trophoblastic cell lines spontaneously secrete interferon-gamma, Placenta 23 (2002) 716–726.
[34] A. Cencic, M. Guillomot, S. Koren, C. La Bonnardiere, Trophoblastic interferons: do they modulate uterine cellular markers at the time of conceptus attachment in the pig? Placenta 24 (2003) 862–869.
[35] C. Davy, J. Doorbar, G2/M cell cycle arrest in the life cycle of viruses, Virology 368 (2007) 219–226.
[36] J.A. Ferreira Barbosa, J. Labrie, F. Beaudry, C.A. Gagnon, M. Jacques, Actinobacillus pleuropneumoniae induces SJPL cell cycle arrest in G2/M-phase and inhibits porcine reproductive and respiratory syndrome virus replication, Virol. J. 12 (2015) 188, https://doi.org/10.1186/s12985-015-0404-3.
[37] M. Bidarimath, K. Khalaj, R.T. Kridli, F.W. Kan, M. Koti, C. Tayade, Extracellular vesicle mediated intercellular communication at the porcine maternal-fetal interface: a new paradigm for conceptus-endometrial cross-talk, Sci. Rep. 7 (2017) 40476, https://doi.org/10.1038/srep40476.
[38] H. Valadi, K. Ekstrom, A. Bossios, M. Sjostrand, J.J. Lee, J.O. Lotvall, Exosome-mediated transfer of mRNAs and microRNAs is a novel mechanism of genetic exchange between cells, Nat. Cell Biol. 9 (2007) 654–659.
[39] T. Wang, L. Fang, F. Zhao, D. Wang, S. Xiao, Exosomes mediate intercellular transmission of porcine reproductive and respiratory syndrome virus, J. Virol. 92 (2018), https://doi.org/10.1128/JVI.01734-17 e01734-17.
[40] S. Montaner-Tarbes, F.E. Borras, M. Montoya, L. Fraile, H.A. Del Portillo, Serum-derived exosomes from non-viremic animals previously exposed to the porcine respiratory and reproductive virus contain antigenic viral proteins, Vet. Res. 47 (2016) 59, https://doi.org/10.1186/s13567-016-0345-x.